Photodissociation dynamics of dimethyl sulfoxide-d6 at 210 nm: Experimental evidence for a prompt anisotropic CD3 channel

ARTICLE *in* CHEMICAL PHYSICS LETTERS · MARCH 2004

Impact Factor: 1.9 · DOI: 10.1016/j.cplett.2004.01.091

5 AUTHORS, INCLUDING:

Isayana Torres
Universidad Nacional de Ingeniería (Nicara…
40 PUBLICATIONS **1,511** CITATIONS
SEE PROFILE

Gustavo A Pino
Universidad Nacional de Córdoba and CON…
35 PUBLICATIONS **327** CITATIONS
SEE PROFILE

Available online at www.sciencedirect.com
SCIENCE DIRECT®
Chemical Physics Letters 386 (2004) 419–424
CHEMICAL PHYSICS LETTERS
www.elsevier.com/locate/cplett

Photodissociation dynamics of dimethyl sulfoxide-d_6 at 210 nm: experimental evidence for a prompt anisotropic CD_3 channel

G.A. Amaral, I. Torres, G.A. Pino, F.J. Aoiz, L. Bañares *

Departamento de Química Física, Facultad de Química, Universidad Complutense de Madrid, 28040 Madrid, Spain

Received 15 December 2003; in final form 20 January 2004

Abstract

The photodissociation of dimethyl sulfoxide-d_6 has been studied at 210 nm by REMPI-TOFMS spectroscopy. The anisotropy of a fast CD_3 dissociation channel has been characterized for the first time. This channel corresponds to the formation of CD_3 and electronically excited $CD_3SO(\tilde{A})$ with an anisotropy parameter $\beta = 0.28 \pm 0.05$. About 38% of the primary CD_3 fragments are formed via this fast dissociative channel with a large translational energy release. A slow isotropic primary CD_3 channel as well as a secondary CD_3 channel arising from internally hot $CD_3SO(\tilde{X})$ have been detected in accordance to previous studies at 210 nm.

1. Introduction

The UV photodissociation of dimethyl sulfoxide (DMSO) has been studied in the past due to its interesting dynamical properties. DMSO is the sulfur analog of acetone and its photodissociation is a source of CD_3 fragments according to:

$$CD_3SOCD_3 + h\nu \rightarrow CD_3 + CD_3SO(\tilde{X}) \quad \Delta H^0 = 218 \text{ kJ/mol} \tag{1}$$

The $CD_3SO(\tilde{X})$ fragment can undergo secondary dissociation according to:

$$CD_3SO(\tilde{X}) \rightarrow CD_3 + SO \qquad \Delta H^0 = 213 \text{ kJ/mol} \tag{2}$$

As in acetone photodissociation, reaction (2) has received a considerable attention in the past [1–5]. Reaction (2) can occur after step (1) has been completed (stepwise mechanism) or concurrently to it (concerted mechanism), thus representing a challenge from both experimental and theoretical points of view. Chen et al. [1] studied DMSO photodissociation at 193 nm using resonance enhanced multiphoton ionization (REMPI) with time-of-flight mass spectrometry (TOFMS). They measured a quantum yield of 1 for the SO fragment by laser induced fluorescence (LIF), and this was taken as an evidence for a concerted dissociation mechanism. However, in later experiments also at 193 nm by Zhao et al. [2] and Rudolph et al. [3] using different techniques, quantum yields of 1.5 and 1.4 for CH_3 and CD_3, respectively, were obtained, indicating a stepwise mechanism in which only part of the CH_3SO/CD_3SO fragments produced in (1) undergoes secondary dissociation. Zhao et al. [2] also found that the angular distribution of the fragments were isotropic. Simultaneously, Blank et al. [4] performed photodissociation studies of DMSO by photofragment translational spectroscopy and deduced that most of the dissociation occurs in a stepwise fashion in agreement with Zhao et al. and Rudolph et al. Three different types of CD_3 fragments were experimentally observed: (i) those corresponding to reaction (1) formed via internal conversion (IC) from the excited state to the ground state of DMSO, (ii) those arising from reaction:

$$CD_3SOCD_3 + h\nu \rightarrow CD_3 + CD_3SO(\tilde{A}) \tag{3}$$

in which the CD_3SO fragments are presumably formed in its first electronically excited state, and (iii) those arising from the unimolecular decomposition of the ground state $CD_3SO(\tilde{X})$ fragment according to (2). However, all three angular distributions of the CD_3

* Corresponding author. Fax: +34-913944135.
E-mail address: banares@legendre.quim.ucm.es (L. Bañares).

0009-2614/$ - see front matter © 2004 Elsevier B.V. All rights reserved.
doi:10.1016/j.cplett.2004.01.091

fragments appeared to be isotropic, despite the fact that the authors of [4] expected that type (ii) CD_3 fragments show a slight anisotropy. Thorson et al. [5] obtained similar results at 210 and 222 nm, but they did not detect CD_3 fragments from reaction (3). They also observed an increase on the yield of CD_3 fragments from reaction (2) as the excitation wavelength was decreased from 222 to 210 nm.

In this Letter, we present careful measurements of TOF profiles at different polarizations of the photolysis laser that have allowed us the identification and characterization of a prompt anisotropic channel in the photodissociation of DMSO-d_6 at 210 nm.

2. Experimental

The experimental setup has been described in detail elsewhere [6]. Briefly, it consists of a supersonic jet chamber (10^{-6} Torr, under operation conditions) where the jet is entrained perpendicular to the laser beams as well as to the TOF direction towards a microchannel plate (MCP) detector. The two laser beams (photolysis and probe beams) are counterpropagated into the chamber where they overlap and meet the jet at the ionization point. Ions are extracted from the interaction region using continuous voltages applied to a series of stainless steel plates that are arranged in a Wiley–McLaren [7] type setup under space focusing conditions.

The supersonic jet is produced by the co-expansion of DMSO-d_6 (Aldrich, 99.0%, room temperature) and He through a pulsed valve (General Valve, No. 9) 0.5 mm diameter nozzle, into the chamber (stagnation pressure ≈200 Torr). The jet is intercepted by the photolysis laser beam ($\lambda = 210$ nm) first and 18–90 ns later by the probe laser beam, which ionizes the CD_3 fragments via a 2 + 1 REMPI scheme on the $4p_z\,^2A_2'' \leftarrow \tilde{X}^2A_2''$ transition (Q 0_0^0, 286.6 nm). The photolysis laser is fired at an optimal time (≈200 μs) after the pulsed valve, interacting with the early edge of the jet where cluster formation is minimized. The photolysis laser is the frequency-mixed output of a 532 nm Nd:YAG (Quanta Ray Pro 230) laser-pumped dye laser (Continuum ND 60) operating at 630 nm. The probe laser is the frequency-doubled tunable output of a 532 nm Nd:YAG (Continuum NY 81) laser-pumped dye laser (Continuum ND 60) operating around 573.3 nm. Both lasers are linearly polarized. The photolysis laser polarization plane may be rotated by inserting a double Fresnel rhomb in the beam path before entering the jet chamber. Typically, the photolysis laser was used at energies $\leqslant 10$ μJ/pulse focused to a spot of ≈0.2 mm diameter, whereas the probe laser was used at energies of 300–600 μJ/pulse focused to a spot of ≈0.3 mm diameter. Both lasers as well as the pulsed valve were operated at a frequency of 10 Hz.

3. Results and discussion

Fig. 1 shows the absorption spectrum of DMSO-d_6. At 210 nm, two absorption bands carry the oscillator strength, the major component being the allowed $\sigma^* \leftarrow$ n (or d ← n) transition with a minor component from the forbidden $\pi^* \leftarrow$ n. It is worth noticing that at this wavelength there is little contribution from the stronger $\pi^* \leftarrow \pi$ band, which is the responsible for the absorption at 193 nm where the majority of the previous DMSO studies were performed. Fig. 1b shows that at 210 nm the available energy is enough to produce one or two CD_3 fragments.

The mass spectrum obtained following DMSO-d_6 photodissociation at 210 nm shows several fragment ions when the probe laser is tuned to the REMPI rotational line R(5) of the CD_3 fragment. After subtraction

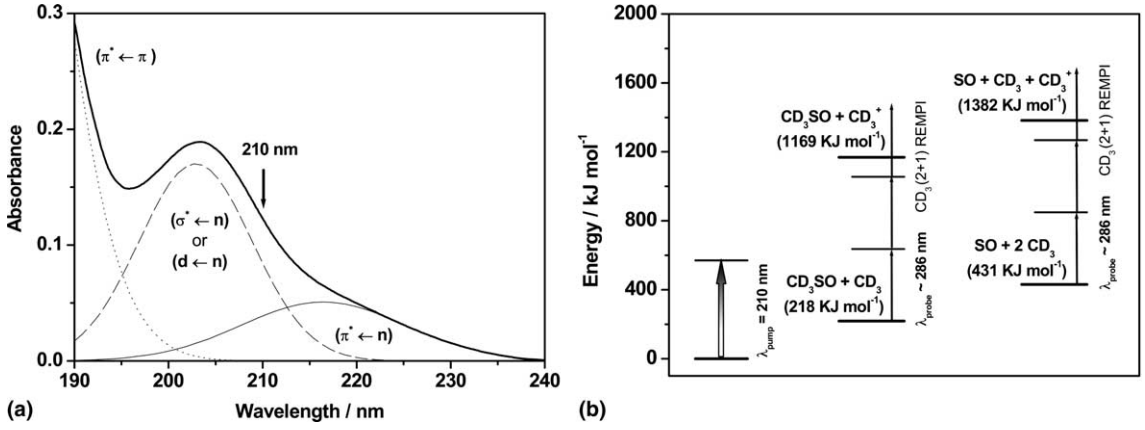

Fig. 1. (a) Gas phase DMSO-d_6 absorption spectrum (bold solid line) deconvoluted in three electronic transitions; solid line: not allowed ($\pi^* \leftarrow$ n) transition, dashed line: either ($\sigma^* \leftarrow$ n) or (d ← n) allowed transition and dotted line: ($\pi^* \leftarrow \pi$) allowed transition. The arrow in the figure indicates the photolysis wavelength studied in this work. (b) Energy level diagram of the two dissociation channels producing CD_3 fragments. The detection REMPI scheme of the CD_3 photofragment for the $4p_z\,^2A_2'' \leftarrow XA_2''$ transition is also displayed.

of the separate contributions from the photolysis and probe lasers alone, there are several types of fragments that exhibit pure pump–probe signals at certain pump–probe delays. Fig. 2 shows the intensity of the pump–probe signal as a function of the time delay between the pump and probe laser beams for the three more important fragment ions observed in the present study: CD_3^+, CD_3SO^+ and SO^+/CD_2S^+. When both lasers overlap in time, there is a sharp increase in the CD_3^+ signal as well as the appearance of the CD_3SO^+ and SO^+/CD_2S^+ fragments. A power dependence study shows that the intensity of the CD_3^+ signal depends linearly on the photolysis laser fluence thus indicating that all CD_3 fragments probed in our experiments arise from one photolysis photon processes. In any case, we have worked under very low photolysis ($\leqslant$10 μJ/pulse) and probe (300–600 μJ/pulse) laser powers and at time delays between the photolysis and probe lasers, $\Delta\tau$, larger than 18 ns (shaded area in Fig. 2) to avoid multiple photon absorptions.

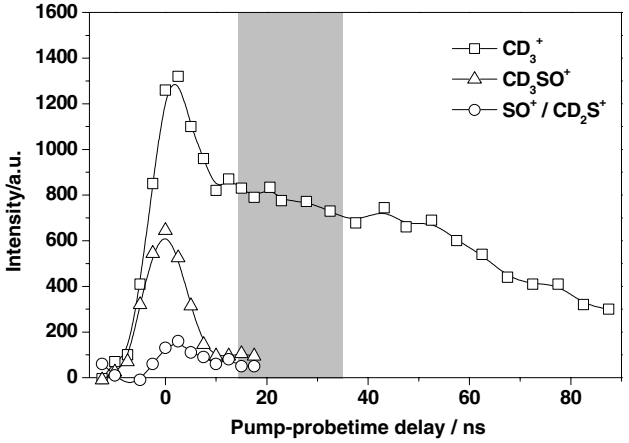

Fig. 2. Pump–probe signal intensity of different fragment ions as a function of the pump–probe time delay. The sharp peaks at near zero time delay arise from non-resonant MPI processes when the two lasers overlap in time. The shaded area corresponds to the time delays used in the experiments. The probe laser was tuned at the R(5) rotational line of the CD_3 species.

The widths of the features in the TOF mass spectrum reveal the recoil energy of the detected fragments. By turning down both the repulsive and extraction voltages (300 and 240 V, respectively), we can accomplish a better separation between ions with different initial velocities, but we are also limited by the ion loss. The ion loss at our working conditions has been estimated to be less than 1.5% using the ion trajectory simulation program SIMION-3D [8].

Fig. 3 shows TOF profiles (expressed as $t - t_0$ with t_0 being the center of the profile) at mass 18 measured at different time delays $\Delta\tau$ and with the probe laser tuned at the Q 0_0^0 branch of the CD_3 $4p_z$ transition. Special attention was paid to guarantee that the Q-branch signal was not saturated. It must be pointed out that the raw TOF profiles were slightly asymmetric about t_0 and that a symmetrization procedure was applied by averaging the left and right parts of each profile with respect to t_0 in order to obtain the TOF profiles shown in Fig. 3. At each time delay, $\Delta\tau$, two different photolysis laser

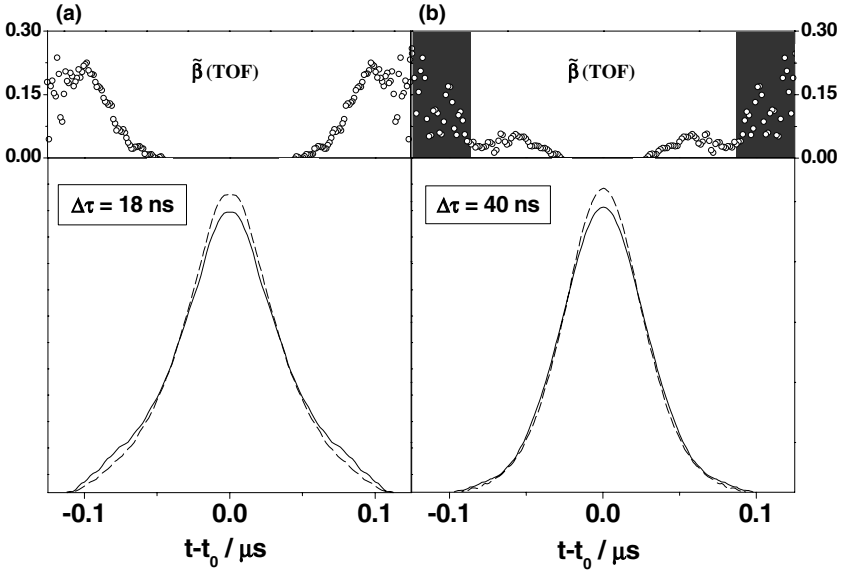

Fig. 3. (a) Top panel: experimental velocity dependent $\tilde{\beta}$(TOF) function for the Q 0_0^0 line of the CD_3 $4p_z$ transition at two different time delays as calculated using Eq. (4). Bottom panel: experimental TOF profiles at perpendicular (dashed line) and parallel (solid line) polarizations of the photolysis laser with respect to the TOF direction. (b) Same as above but at 40 ns time delay. The shaded part in (b) shows the area in which the noise prevents a reliable determination of $\tilde{\beta}$(TOF).

polarization orientation spectra are shown according to whether the polarization plane of the photolysis laser is parallel or perpendicular to the TOF (recoil) axis (Z-axis). Special care was taken in the measurements to ensure that the difference in the area of the TOF profiles at each photolysis laser polarization was not larger than 1.5% (see above), in order to achieve identical or similar detection sensitivities, thus avoiding any further normalization. At small $\Delta\tau$ the TOF profiles for the parallel and perpendicular polarizations differ on both sides of the profile, suggesting an anisotropic behavior for those CD_3 fragments that arrive at small (negative $t - t_0$) and large (positive $t - t_0$) times. These ions correspond to those CD_3 fragments with maximum absolute value of Z-axis velocity component $|v_Z|$. As $\Delta\tau$ increases, the faster fragments produced in the photolysis escape from the interaction region, and are increasingly missed by the probe laser. This effect can be appreciated in Fig. 3 where the fast anisotropic portion of the TOF profiles diminishes from 18 to 40 ns time delays. To our knowledge this anisotropy has not been detected in previous experiments. Thorson et al. [5] also worked at 210 nm, but they did not observe any anisotropy in their measurements mostly due to the fact that they were working at pump–probe time delays of 100 ns where most of the fast anisotropic CD_3 fragments had escaped from the interaction region.

Since in the present case the anisotropy is determined as a function of v_Z instead of v, an actual anisotropy parameter β cannot be determined for the whole range of speeds. However, an 'anisotropy function' $\tilde{\beta}$(TOF) as a function of the time-of-flight can be defined as:

$$\tilde{\beta}(\mathrm{TOF}) = \frac{2\left[I_{\parallel}(\mathrm{TOF}) - I_{\perp}(\mathrm{TOF})\right]}{\left[I_{\parallel}(\mathrm{TOF}) + 2I_{\perp}(\mathrm{TOF})\right]}, \tag{4}$$

where $I_{\parallel}$(TOF) and $I_{\perp}$(TOF) are the signal intensities measured when the photolysis laser is polarized parallel or perpendicular to the TOF axis, respectively. The physical meaning of $\tilde{\beta}$(TOF) is that of an average of the actual β over all speeds v with a given v_Z projection. Therefore, although $\tilde{\beta}$(TOF) is calculated using the same formula as the anisotropy parameter β [9,10], it does not contain the same information. Only for those fragments arriving at the largest $|t - t_0|$, when $v_Z \approx v$, the values of $\tilde{\beta}$(TOF) are a good approximation to the actual values of the anisotropy parameter β . Note that the negative values of $\tilde{\beta}$(TOF) arround $|t - t_0| \approx 0$ do not necessarily imply a negative value of the β parameter. In addition, $\tilde{\beta}$(TOF) is strongly dependent on the shape of the velocity distributions used to fit the experimental data. Finally, had all CD_3 channels been isotropic, $\tilde{\beta}$(TOF) should have been zero for the entire distribution, a fact which is clearly not observed.

The maximum positive value of $\tilde{\beta}$(TOF) ($\sim$0.23) at 18 ns time delay for the anisotropic part of the signal indicates a parallel transition. At larger time delays, the value of $\tilde{\beta}$(TOF) decreases because the fast anisotropic CD_3 fragments escape from the ionization region. TOF profiles can be fitted as the weighted sum of different CD_3 contributions, with the total sum being the convolution of the instrumental response function over the projected velocity distribution on the detector axis, $f(v_z, \theta)$ [11]. In the absence of angular momentum alignment of the fragments, the projected velocity distribution on the detector axis observed experimentally is given by:

$$f(v_z, \theta) = \sum_i C_i \int_{|v_z|}^{v_{\max}} \frac{g_i(v)}{2v} \left\{1 + \beta_i P_2(\cos\theta) P_2\left(\frac{v_z}{v}\right)\right\} \mathrm{d}v, \tag{5}$$

where $g_i(v)$ are the normalized velocity distributions of the neutral fragments in the center-of-mass (CM) frame for each of the CD_3 channels, C_i their fraction contribution to the total signal and β_i are their corresponding anisotropy parameters. Under space-focusing conditions, v_z can be calculated as:

$$v_Z = \frac{q}{m} E_{\mathrm{EXT}}(t - t_0), \tag{6}$$

where t is the ion arrival time, q/m is the charge-to-mass ratio of the detected ion, E_{EXT} is the extraction electric field, and t_0 is the mean flight time of the ion.

The fitting procedure began with the TOF profile analysis at both laser polarizations by means of Eq. (5). At first we tried to fit the profiles with two different components: an isotropic Boltzmann velocity distribution and an anisotropic distribution built from a center-of-mass (CM) recoil energy distribution, $P(E)$, modeled by a modified Gaussian function of the form [11]:

$$P(E) = NE^{3/2}(E_{\max} - E) \exp\left(-\left(\frac{E - E_0}{\Delta E}\right)^2\right), \tag{7}$$

which is typical of a fast dissociation with a large translational energy release. The fitting parameters were the Boltzmann distribution temperature, the width and center of the modified Gaussian distribution and the contribution C_i for each component. The value of $E_{\max}$ in the latter is fixed at the energy corresponding to the maximum observed time in the TOF profiles. For the anisotropic channel, β was initially fixed at 0.23, which is the maximum value observed in the $\tilde{\beta}$(TOF) shown in Fig. 3. However, since the maximum $\tilde{\beta}$(TOF) value can only be taken as a lower limit for β, it was also later used as a fitting parameter. Despite the wealth of parameter combinations tried in this fitting procedure we could never achieve good agreement with the experimental TOF distributions for both polarizations as well as the $\tilde{\beta}$(TOF) function.

Much better results were obtained when an isotropic Gaussian distribution was added as a third component to the overall fitting procedure. Blank et al. [4] had observed a second isotropic type of CD_3 fragments at

193 nm, attributed to the secondary dissociation of the internally hot $CD_3SO(\tilde{X})$ fragment. They postulated an exit barrier for this channel of about 33.5 kJ/mol, which, in principle should yield a Gaussian type CM energy distribution.

Fig. 4 shows the very good agreement found between the best fit and the actual TOF as well as for the $\tilde{\beta}$(TOF). From the TOF profiles fittings we can calculate the separate CD_3 energy distributions in the CM frame, which in turn can be converted to CM translational energy distributions for each channel, as shown in Fig. 5. It is clear that the modified Gaussian distribution dominates the CD_3 distribution at large $|t - t_0|$. Table 1 shows the calculated CM mean translational energy as well as the best C_i values obtained for each of the three contributions involved in the fitting. The results obtained from the simulation of the symmetrized TOF profiles are exactly the average between the values determined from the simulations of the left and the right parts of the slightly asymmetric raw data separately. The errors that can be introduced by the symmetrization procedure are within the uncertainties of the parameters characterizing the center-of-mass kinetic energy distributions of the different channels. It is clear that the major channel in the photodissociation corresponds to the Boltzmann type contribution component with an average translational energy of 19.8 ± 0.4 kJ/mol. Due to its statistical behavior, we believe that it corresponds

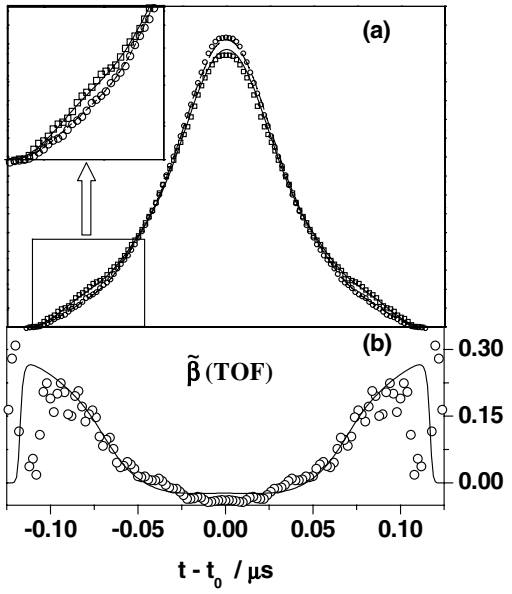

Fig. 4. (a) Experimental (symbols) and simulated (lines) TOF profiles of the Q 0_0^0 line of the CD_3 $4p_z$ transition using parallel (squares and solid line) or perpendicular (circles and dashed line) polarized photolysis light. The inset on the top left part of the figure zooms in the signal portion corresponding to fast ions directed initially to the detector. (b) Velocity dependent anisotropy function $\tilde{\beta}$(TOF) calculated with equation [4] using the experimental (circles) and simulated (solid line) TOF profiles.

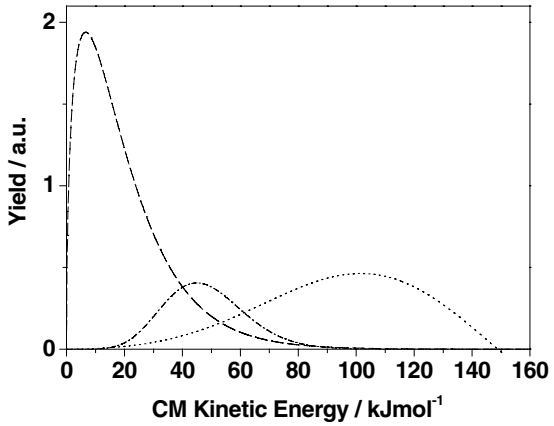

Fig. 5. Best fit CM kinetic energy distributions after dissociation of DMSO-d_6 at 210 nm. Dashed line: Boltzmann isotropic distribution; dotted line: Modified Gaussian anisotropic distribution ($\beta = 0.28$) and dashed-dotted line: Gaussian isotropic distribution. Each distribution is multiplied by its relative contribution, C_i.

Table 1
Fraction of the total signal, C_i, anistotropy parameter, β_i, and center-of-mass mean translational energy, $\langle E_T \rangle$, for the different contributions

	Function type		
	Boltzmann	Modified Gaussian	Gaussian
$C_i \pm 0.01$	0.53	0.33	0.14
$\beta_i \pm 0.05$	0	0.28	0
$\langle E_T \rangle$ (kJ mol^{-1})	19.8 ± 0.4	94 ± 4	48.1 ± 0.1

to CD_3 fragments that arise from the unimolecular dissociation of internally hot ground state DMSO-d_6 formed by internal conversion (IC) from the excited state (the overall process corresponding to reaction (1)). The other primary CD_3 channel is the fast anisotropic distribution with a mean translational energy of 94 ± 4 kJ/mol and an anisotropy parameter $\beta = 0.28 \pm 0.05$, which we assign to process (3) where electronically excited $CD_3SO(\tilde{A})$ fragments are produced. Taking into account that the latter has a $C_i = 0.33$, we conclude that 38% of the DMSO-d_6 undergoes primary fast CD_3 dissociation which is larger than the 27% measured by Blank et al. [4] at 193 nm. Finally, the Gaussian energy distribution peaking at 45 kJ/mol is assigned to the secondary dissociation of internally hot $CD_3SO(\tilde{X})$ fragments formed in process (1). Its $C_i = 0.14$ renders a CD_3 quantum yield of 1.2, slightly smaller than the value of 1.3 measured by Thorson et al. [5] at 210 nm.

According to the present data, the electronically excited state of $CD_3SO(\tilde{A})$ lies 203 ± 8 kJ/mol above the ground state, [1] in agreement with Blank et al. [4] who postulated a value of 225 kJ/mol. The present value

[1] This value has been obtained as the difference between the available energy (351.8 kJ/mol) and the maximum recoil energy of the modified Gaussian anisotropic distribution shown in Fig. 5 (148.9 kJ/mol).

gives a translational energy release of $\langle f_T \rangle = 0.63$ for channel (3), consistent either with a direct dissociation on a repulsive electronic surface or electronic predissociation on a surface with a large barrier to recombination. The relatively small amount of fast anisotropic fragments observed suggests, however, that the most likely mechanism for the fast primary photodissociation is electronic predissociation involving a repulsive potential surface that correlates adiabatically with electronically excited $CD_3SO(\tilde{A})$.

4. Conclusions

We have been able to detect a fast anisotropic CD_3 channel in the photolysis of DMSO-d_6 at 210 nm for the first time. The anisotropy parameter $\beta = 0.28 \pm 0.05$ is consistent with a parallel transition with the transition dipole moment within the CSCO plane in C_{2v} geometry. The energy balance indicates that the fast channel corresponds to the formation of CD_3 in its ground state plus an electronically excited state of $CD_3SO(\tilde{A})$ according to reaction (3). Thirty eight percent of the primary dissociation occurs via this fast dissociation with a translational energy release of 63% of the available energy, which suggests that the mechanism is consistent with predissociation from the excited state to a repulsive surface without an exit barrier. The latter is also consistent with the data at 193 nm, in which 62% of the available energy appears as translational energy in the products. Further studies are underway to explore the behavior of this fast channel at different photolysis wavelengths in the range of 204–227 nm. Furthermore, we are also extending the study at 210 nm to unravel the energy partitioning in the products, particularly rotational and vibrational energy of the different CD_3 fragments.

The results obtained for the slow primary CD_3 channel as well as the secondary dissociation of internally hot $CD_3SO(\tilde{X})$ are consistent with previous studies at 210 nm [5] as well as 193 nm [3,4].

Acknowledgements

G.A.M. and G.A.P. gratefully acknowledge finantial support from the Spanish MECD through the State Secretary of Education and Universities. I.T. thanks the Spanish Ministry of Science and Technology for financial support within the programme 'Ramón y Cajal'. The project has been financed by DGES of Spain under project BQU2002-04627-C02-02 and by the EU RTN 'Reaction Dynamics' HPRN-CT-1999-00007. The facilities provided by the CAI de Espectroscopía Multifotónica of the Universidad Complutense are gratefully acknowledged.

References

[1] X. Chen, F. Asmar, H. Wang, B.R. Weiner, J. Phys. Chem. 95 (1991) 6415.
[2] H.Q. Zhao, Y.S. Cheung, D.P. Heck, C.Y. Ng, T. Tetzlaff, W.S. Jenks, J. Chem. Phys. 106 (1997) 86.
[3] R.N. Rudolph, S.W. North, G.E. Hall, T.J. Sears, J. Chem. Phys. 106 (1997) 1346.
[4] D.A. Blank, S.W. North, D. Stranges, A.G. Suits, Y.T. Lee, J. Chem. Phys. 106 (1997) 539.
[5] G.M. Thorson, Ch.M. Cheatum, M.J. Coffey, F.F. Crim, J. Chem. Phys. 110 (1999) 10843.
[6] J. Barr, I. Torres, L. Bañares, J.E. Verdasco, F.J. Aoiz, Chem. Phys. Lett. 373 (2003) 550.
[7] W.C. Wiley, I.H. McLaren, Rev. Sci. Instr. 26 (1955) 1150.
[8] Simion 3-D, Versión 6.0, Idaho National Engineering Laboratory, EG&G Idaho Inc., Idaho Falls, ID., 1987.
[9] R.N. Zare, Mol. Photochem. 4 (1972) 1.
[10] G. Amaral, K. Xu, J. Zhang, J. Phys. Chem. A 105 (2001) 1465.
[11] B. Martínez-Haya, F.J. Aoiz, L. Bañares, P. Quintana, E. Verdasco, J. Phys. Chem. A 104 (2000) 10150.